



DriPE: A Dataset for Human Pose Estimation in Real-World Driving Settings

Romain Guesdon, Carlos F Crispim-Junior, Laure Tougne

► To cite this version:

Romain Guesdon, Carlos F Crispim-Junior, Laure Tougne. DriPE: A Dataset for Human Pose Estimation in Real-World Driving Settings. 2nd Autonomous Vehicle Vision (AVVision) - International Conference on Computer Vision (ICCV) Workshop, Oct 2021, Virtual Conference, France. 10.1109/ICCVW54120.2021.00321 . hal-03380579

HAL Id: hal-03380579

<https://hal.science/hal-03380579>

Submitted on 15 Oct 2021

HAL is a multi-disciplinary open access archive for the deposit and dissemination of scientific research documents, whether they are published or not. The documents may come from teaching and research institutions in France or abroad, or from public or private research centers.

L'archive ouverte pluridisciplinaire **HAL**, est destinée au dépôt et à la diffusion de documents scientifiques de niveau recherche, publiés ou non, émanant des établissements d'enseignement et de recherche français ou étrangers, des laboratoires publics ou privés.

DriPE: A Dataset for Human Pose Estimation in Real-World Driving Settings

Romain Guesdon

Carlos Crispim-Junior
Univ Lyon, Lyon 2, LIRIS
Lyon, France, F-69676

Laure Tougne

{romain.guesdon, carlos.crispim-junior, laure.tougne} @liris.cnrs.fr

Abstract

1 *The task of 2D human pose estimation has known a significant gain of performance with the advent of deep learning.*
2 *This task aims to estimate the body keypoints of people in*
3 *an image or a video. However, real-life applications of such*
4 *methods bring new challenges that are under-represented*
5 *in the general context datasets. For instance, driver sta-*
6 *tus monitoring on consumer road vehicles introduces new*
7 *difficulties, like self- and background body-part occlusions,*
8 *varying illumination conditions, cramped view angles, etc.*
9 *These monitoring conditions are currently absent in general*
10 *purposes datasets. This paper proposes two main contribu-*
11 *tions. Firstly, we introduce DriPE (Driver Pose Estimation),*
12 *a new dataset to foster the development and evaluation of*
13 *methods for human pose estimation of drivers in consumer*
14 *vehicles. This is the first publicly available dataset depicting*
15 *drivers in real scenes. It contains 10k images of 19 different*
16 *driver subjects, manually annotated with human body key-*
17 *points and an object bounding box. Secondly, we propose a*
18 *new keypoint-based metric for human pose estimation. This*
19 *metric highlights the limitations of current metrics for HPE*
20 *evaluation and of current deep neural networks on pose*
21 *estimation, both on general and driving-related datasets.*

35 applications, *e.g.*, strong body occlusion or varying illumination.
36

37 Pose estimation inside of a vehicle brings new difficulties
38 that are under-represented in general datasets (Fig. 1). First,
39 the camera placement causes a strong side viewing angle,
40 producing both self- and background occlusion (*e.g.*, by the
41 dashboard and the wheel). By consequence, the side of the
42 subject’s body opposite to the camera becomes more difficult
43 to detect (Fig. 1C). Luminance is also an important factor
44 in HPE. For instance, body parts can be fully visible in a
45 regular pose but be missed by the network due to strong
46 illumination (Fig. 1A). Also, the outside light may visually
47 split the upper body into two halves, and hence deceive the
48 network (Fig. 1B). Finally, the low contrast of the car interior
49 can make the detection of body parts difficult, like the right
50 forearm in the picture (Fig. 1D), depending on the color
51 of the subject’s clothes. To evaluate the open challenges
52 on human pose estimation in consumer cars, we propose
53 the first publicly-available dataset in real-world conditions
54 called DriPE (Driver Pose Estimation)¹.

55 Moreover, we study the limitations of existing metrics
56 [12, 24, 40] for the evaluation of the HPE task on keypoint
57 detection, on both general and driving contexts. Based on
58 our observations, we propose a new metric called mAPK to
59 characterize the observed limitations. This metric is essential
60 to highlight the challenges presented by DriPE, and up to
61 now ignored in general datasets, such as background and
62 self-occlusion.

63 This paper is organized as follows. Section 2 presents
64 related work on human pose estimation. In Section 3, we
65 present DriPE dataset. We describe in Section 4 the proposed
66 mAPK metric. Section 5 introduces the evaluated networks
67 and describes their architecture. We present and discuss
68 in Section 6 the experimental results. Finally, Section 7
69 presents our conclusions and future work.

¹DriPE dataset is publicly available on: https://gitlab.liris.cnrs.fr/aura_autobehave/dripe

1. Introduction

24 Human Pose Estimation (HPE) is a well-known task in
25 computer vision. This problem aims to find the position
26 of keypoints in the 2D plane or the 3D space. Keypoints
27 are generally placed on the body joints (shoulders, elbows,
28 wrists, hips, knees, ankles), and the head. Additional points
29 can be placed on hands, feet, or face.

30 State-of-the-art methods have reached good performances
31 on HPE challenges on both single-person [1, 19, 30] and
32 multiperson datasets [24], especially through deep learn-
33 ing. However, these general-purpose datasets do not depict
34 challenging scenes that might occur very often in real-life

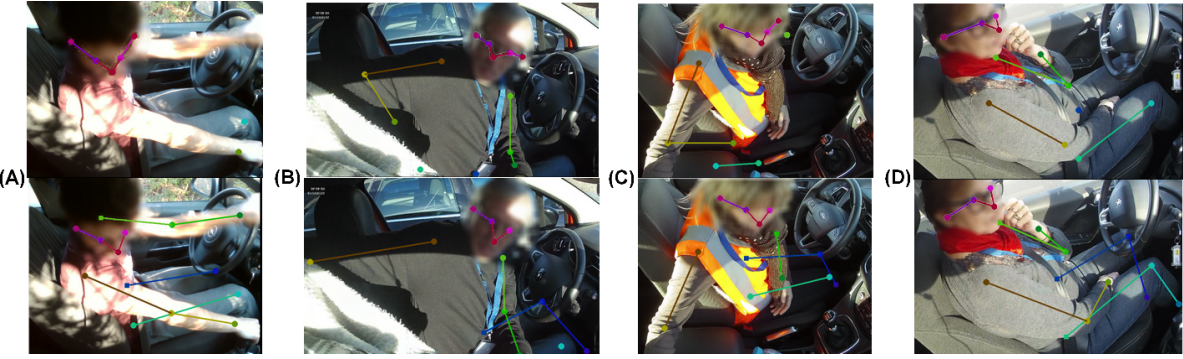


Figure 1: Samples of DriPE dataset. The top and bottom rows show, respectively, pose predictions by Simple Baseline network [39] and ground truth data. Faces have been blurred on this figure to anonymize the participants’ identities.

2. Related Work

This section presents the work related to keypoint detection for human pose estimation. More precisely, we discuss the datasets used for this task, the current methods for pose estimation, and the metrics used to evaluate their accuracy.

2.1. Datasets

Datasets play an important role in the performance of deep learning methods. Improvements in the human pose estimation using deep learning networks have been partly justified by new datasets with more subjects’ pictures and more variability in their poses, the angles of view, the background, etc.

Leeds Sports Pose (LSP) [19] dataset is the first HPE dataset released with more than 1k training images, which was later extended to 11k. It contains pictures of full-body subjects practicing different sports extracted from Flickr. Frames Labeled In Cinema (FLIC) dataset [30] is formed of around 5k pictures extracted from Hollywood movies. The Max Planck Institute for Informatics (MPII) dataset [1] contains around 25k images extracted from various YouTube videos. Microsoft Common Objects in Context (COCO) [24] is originally an object detection and segmentation dataset, which was then expanded to a multiperson HPE dataset. It is composed of more than 250k pictures extracted from Bing, Flickr, and Google.

Even if these general datasets can be useful for training or benchmarking, they might not present certain challenging situations that might occur in domain-specific datasets. Therefore, several datasets have been published in the last years focusing on monitoring people inside cars [3, 4, 13, 18, 25]. However, they are mostly focused on the action recognition task. Furthermore, most of the available datasets are recorded in studios and do not represent natural foreground nor illumination changes present in vehicle cockpit during a daily routine ride, which are true challenges for HPE methods. For instance, authors in [25] propose Drive&Act dataset,

depicting multi-view and multi-modal (RGB, NIR, depth) actions in a static driving simulator, with labeled actions and predicted 3D human poses. DFKI [13] describes a new test platform to record in-cabin scenes. However, no public dataset for HPE in a vehicle using this setup has been recorded or published up to now.

Besides, HPE datasets do not use exactly the same keypoints to represent the body. Most of the representations, commonly called skeletons, include one joint marker per major body limb articulation (shoulder, elbow, wrist, hip, knee, ankle). However, while some datasets [1, 19] only put markers on the top of the head and the base of the neck, others adopt a finer representation (eyes, nose, ears) [24]. Some works also extend the human pose representation to hands and feet [16, 6].

In the end, the most prominent general datasets in the state of the art of HPE are MPII [1] and LSP [19] for single-person and COCO [24] for multiperson pose estimation. Regarding the pose estimation inside of a vehicle, there is no publicly available dataset for HPE which presents real driving conditions.

2.2. HPE Methods

The pose estimation methods may be divided into two types: single-person and multiperson methods.

2.2.1 Single-person Pose Estimation

Single-person methods for HPE using convolutional neural networks can be split into two categories: regression-based and detection-based methods.

Regression-based CNN methods aim to directly predict the keypoints coordinates from pictures. AlexNet [21] is the first CNN baseline used for HPE. Toshev and Szegedy [36] use AlexNet as a multi-stage coordinate estimator and refiner. Carreira *et al.* [8] propose an Iterative Error Feedback network based on the deep convolution network GoogleNet [33]. Finally, Sun *et al.* [32] propose a parametrized pose repre-

141 sentation using bones instead of keypoints, paired up with 192
142 the ResNet-50 [14] for both 2D and 3D HPE. 193

143 However, regression-based networks usually lack robust- 194
144 ness due to the high non-linearity of the end-to-end structure 195
145 between the image and the coordinates of the keypoints. 196
146 To overcome this issue, many methods have proposed a 197
147 detection-based approach instead. The majority of these 198
148 methods aim to predict heatmaps, *i.e.*, maps where each pixel 199
149 represents the probability for the keypoint to be located here. 200
150 Newell *et al.* [27] propose an architecture composed of new 201
151 modules called Hourglasses, which aim to extract features 202
152 from different scales using a network built based on Residual 203
153 Modules [15]. This architecture has inspired several other 204
154 works [11, 20, 34, 35]. In addition to Hourglass-based meth- 205
155 ods, other detection-based architectures have been developed. 206
156 Chen *et al.* [9] propose an adversarial learning architecture 207
157 that combines a heatmap pose generator with two discrimina- 208
158 tors. Xiao *et al.* [39] use the ResNet-50 [14] network but add 209
159 deconvolution layers in the last convolution stage to predict 210
160 the heatmaps. Unipose [2] combines a ResNet backbone for 211
161 feature extraction with a waterfall module to perform HPE. 212
162 Sun *et al.* [?] use a parallel multi-scale approach similar to 213
163 the Hourglass with exchange units. 214

164 The networks mentioned previously achieve state-of-the- 215
165 art performances on recent challenges. However, ResNet 216
166 Simple Baseline [39] presents a competitive performance 217
167 while preserving a light architecture compared to others. 218

168 2.2.2 Multiperson Pose Estimation

169 Multiperson HPE brings two difficulties to the problem: find 219
170 the locations of keypoints on the image and associate the 220
171 detected keypoints to the different subjects. Multiperson 221
172 approaches can be divided into two categories: top-down 222
173 and bottom-up methods. 223

174 Top-down approaches first detect the people in the im- 224
175 age and then find the keypoints of each person. Most of 225
176 the top-down methods use a single-person HPE architecture 226
177 preceded by a person detection step: Xiao *et al.* [39] and 227
178 Sun *et al.* [31] both use a faster R-CNN [29] while Chen *et* 228
179 *al.* [10] use a feature pyramid network [23]. Li *et al.* [22] 229
180 propose a multi-stage network with cross-stage feature ag- 230
181 gregation. Cai *et al.* [5] use a similar structure combined 231
182 with an original residual steps block. 232

183 Conversely, bottom-up methods first detect every key- 233
184 point in the image and then infer people instances from them. 234
185 Newell *et al.* [26] reuse their stacked hourglass network for 235
186 single-person HPE and adapt it to multiperson by predict- 236
187 ing an additional association map for each keypoint. Cao 237
188 *et al.* [7] propose an iterative architecture with part affinity 238
189 fields used to associate the keypoints to people. 239

190 Among the described architectures, top-down methods 240
191 currently present the highest performance on HPE. For in-

stance, MSPN [22] and RSN [5] have won the COCO Key- 192
193 point Challenge in 2018 and 2019, respectively. 194

195 2.3. Evaluation Metrics

196 The performances of the general 2D HPE methods can 197
198 be difficult to evaluate since it depends on many criteria 199
199 (number of visible keypoints, number of visible people, size 200
200 of the subjects, etc.). 201

201 One of the first commonly used metrics is Percentage 202
202 of Correct Parts (PCP) [12]. Each keypoint prediction is 203
203 considered correct if its distance to the ground truth is in- 204
204 ferior to a fraction of the limb length (*e.g.*, 0.5). Thereby, 205
205 this metric punishes more severely smaller limbs, which are 206
206 already hard to predict due to their size. To mitigate this 207
207 issue, Percentage of Correct Keypoints (PCK) [40] sets the 208
208 threshold for every keypoint of a subject on a fraction of a 209
209 specific limb’s length. Two thresholds are commonly chosen 210
210 to evaluate the performance in the literature. These metrics 211
211 are mostly employed to evaluate algorithms on single-person 212
212 datasets, like MPII and LSP. 213

213 Another common metric is Average Precision (AP), 214
214 paired up with Average Recall (AR). For single-person net- 215
215 works, APK [40] is computed on keypoint detections. A 216
216 detection is considered as a true positive if it falls under a 217
217 set range of the ground truth, similarly to that PCP and PCK 218
218 metrics, and a false positive otherwise. 219

219 In a multiperson context, most metrics compute the per- 220
220 formance of a method at a person detection level instead of 221
221 a keypoint level. For instance, the mAP metric [1] first pairs 222
222 up each person detection with the ground truth using PCK 223
223 metric. Then, the matched and unmatched people are used 224
224 to compute the average precision and recall. COCO dataset 225
225 proposes a second metric for the evaluation of the HPE task 226
226 that we will refer to as AP OKS. This metric uses the Object 227
227 Keypoint Similarity (OKS) score [24], which is similar to 228
228 the Intersection over Union (IoU), to calculate the distance 229
229 between the people detections and ground truth based on 230
230 keypoints. The final scores are still computed over people. 231

231 One of the main limitations of both PCK and AP OKS 232
232 evaluation metrics is that they both put aside false-positive 233
233 keypoints. Moreover, because the COCO dataset is mostly 234
234 used in a multiperson context, its metric measures precision 235
235 and recall based on people detection, instead of keypoints. 236
236 To address the limitations of previous evaluation procedures, 237
237 we define a new general metric based on keypoints detection 238
238 called mAPK. 239

237 3. DriPE Dataset

238 We propose DriPE, a dataset to evaluate HPE methods 239
239 on real-world driving conditions, containing illumination 240
240 changes, occluding shadows, moving foreground, etc. The 241
241 dataset is composed of 10k pictures of drivers in real-world 242



Figure 2: Image samples from DriPE dataset. Faces on the figure have only been blurred for the purpose of this paper.

	Drive&Act [25]	DriPE
N° subjects	15	19
Female / Male	4 / 11	7 / 12
Annotations	HPE network	Manual
RGB	✓	✓
Depth	✓	-
NIR	✓	-
N° images	9.6M (videos)	10k
Driving context	Simulator	Real world

Table 1: Comparison of driving-related datasets for HPE.

242 conditions, split into 7.4k images for training, and 2.6k images
 243 equally divided into validation and testing sets. Table 1
 244 presents a detailed description of the dataset and compares it
 245 to prior work.

246 3.1. Data Collection

247 To build DriPE, we extracted pictures from videos
 248 recorded during several driving experiments. In each ex-
 249 periment, we installed an RGB camera inside the car on top
 250 of the passenger’s door, directed towards the driver. The
 251 subjects drive either in a real-size replica of a city (closed
 252 track) or on actual roads. In total, we recorded 19 drivers,
 253 allowing us to collect over 100 hours of video clips. We
 254 based the image selection process using two metrics: struc-
 255 tural similarity index measure (SSIM) [37] and brightness
 256 differential. We chose these two metrics with the objec-
 257 tive of extracting pictures with both distinct luminance and
 258 structure. Therefore, we computed the SSIM and the light
 259 differential between two successive frames, with a step of
 260 three frames per second. Then, we selected 10k pictures,
 261 half with the highest absolute light differential, and half with
 262 the lowest SSIM. We defined a minimum time gap between
 263 two selected frames to increase variability.

264 3.2. Annotations

265 We have chosen to follow the COCO dataset’s annota-
 266 tion style for DriPE since face keypoints are particularly
 267 interesting to describe driver attention. For each image, we
 268 annotated the person bounding box and 17 keypoints: arms
 269 and legs with three keypoints each, and 5 additional markers

270 for the eyes, ears, and nose. We split the annotated keypoints
 271 into two categories: visible and non-visible. The non-visible
 272 category corresponds to the occluded points, either by an
 273 object or by the subject body, but which position can still be
 274 deducted from the visible body parts. Note that in this study,
 275 both categories are treated equally by the evaluation methods.
 276 Following the COCO dataset policy, the face keypoints were
 277 annotated only if visible.

278 The ground truth heatmaps were generated using centered
 279 2D Gaussian with a standard deviation of 1px, centered
 280 around the keypoint location.

4. Evaluation Metric

282 Following the state of the art, we only evaluate in this
 283 study detection-based networks, which predict heatmaps.
 284 Each heatmap is a matrix where the elements represent the
 285 probability of a particular keypoint to be located at a pixel.
 286 Therefore, the output of the evaluated network models con-
 287 tains one heatmap per skeleton keypoint. Following the
 288 common practice in 2D single-person HPE [27, 35, 38, 39],
 289 the position of a given keypoint corresponds to the maximum
 290 value of its heatmap. To separate predictions from noise, a
 291 minimum confidence threshold is applied to this maximum.
 292 From these coordinates, several metrics can be calculated to
 293 evaluate the network performances.

294 4.1. Background

295 First, we describe and discuss in detail two evaluation
 296 metrics from the literature: AP OKS and APK.

297 4.1.1 AP OKS

298 To evaluate the performance of each network on the COCO
 299 dataset, the official multiperson metric is based on average
 300 precision (AP) and recall (AR). This evaluation is carried
 301 out following three steps: 1) compute the distance between
 302 each detected person and each ground-truth subject, 2) pair
 303 up the best person detection with its ground-truth, and 3)
 304 compute the precision and recall.

305 The metric used to compute the distance between a per- 349
 306 person's prediction and its ground truth is the OKS (Equation 1). 350

$$\text{OKS} = \frac{\sum_i \text{KS}_i * \delta(v_i > 0)}{\sum_i \delta(v_i > 0)} \quad (1)$$

where KS_i is defined as follows:

$$\text{KS}_i = \exp - \frac{d_i^2}{2.s^2.k_i^2} \quad (2)$$

307 where i iterates over each detected keypoint, d_i is the Eu- 359
 308 clidean distance between the predicted and the ground-truth 360
 309 keypoints, s is the image scale computed from the bounding 361
 310 box size, k_i a per-keypoint constant that tries to homoge- 362
 311 nize the standard deviations between each body part. Non- 363
 312 annotated keypoints have visibility v_i equal to 0, therefore 364
 313 their associated false positives are ignored by OKS computa- 365
 314 tion.

315 Secondly, the OKS scores are used to select the best 366 paired-up people, starting from the highest score. All un- 367 matched detected people or paired-up couples with an OKS 368 score lesser than a selected threshold (ranging from 0.5 to 369
 319 0.95) are discarded. Finally, considering matched and dis- 370
 320 carded people as true and false positives, respectively, the 371
 321 metric computes the mean average precision and recall at a 372
 322 person-level detection.

323 Regarding our problem, this metric has two main limita- 374
 324 tions. Firstly, the OKS metric only considers the annotated 375
 325 body points. This decision prevents the metric to properly 376
 326 measure the keypoint detection's precision of the evaluated 377
 327 methods. This bias can be problematic in contexts where 378
 328 many keypoints cannot be annotated, *e.g.*, in a car context 379
 329 with the strong occlusion (mostly the legs and the bodyside 380
 330 opposite to the camera). Therefore, we want to integrate 381
 331 false-positive keypoints into the performance evaluation of 382
 332 HPE methods. Secondly, the true and false positives are com- 383
 333 puted at the level of person detections instead of keypoints. 384
 334 In summary, this procedure does not properly characterize 385
 335 the performance of the evaluated methods on the task of 386
 336 keypoint detection.

337 4.1.2 APK

338 Average Precision over Keypoints (APK) [40] is a metric 390
 339 that aims to compute precision and recall scores based on 391
 340 keypoints. For each keypoint, a prediction is considered as a 392
 341 true positive if it is located within a defined radial distance 393
 342 from the ground truth. The original work sets this threshold 394
 343 to half the size of the hand. A similar threshold is used to 395
 344 compute Percentage of Correct Keypoints (PCK) [40], and 396
 345 it is defined as a fifth of the torso size (PCK@0.2[19]) or 397
 346 half the head size (PCKh@0.5[19]). Then, non-detected 398
 347 keypoints are counted as false negatives, while points that 399
 348 are detected but not annotated in the ground truth count 399

as false positives. Finally, average precision and recall are 350
 351 computed.

This metric is interesting since it handles the two problems of the COCO OKS metric: it is keypoint-based, and it 352
 353 considers false positives of non-annotated keypoints. This 354
 355 metric has not been used in recent HPE work [2, 20, 34, 39]. 356
 357 One of its main limitations is the use of a distance threshold 358
 359 based on body part size. In fact, the COCO annotation style 360
 361 does not provide hand or head size. The use of the torso 362
 363 is also not an appropriate option in the car cockpit context 364
 365 since, depending on the viewing angle, the torso's full length 366
 367 is not always fully visible on the image.

4.2. mAPK

To address the problems mentioned previously, we propose to compute an evaluation metric based on keypoints 368
 369 instead of people. The mAPK metric reuses the concept from 370
 371 APK of computing average precision and recall based on 372
 373 keypoints but changes the acceptance method. Algorithm 1 374
 375 summarizes the computation process. The algorithm takes as 376
 376 input a list of matched person (gt, dt) from the ground truth 377
 377 and the detection, respectively, as well as two lists represent- 378
 378 ing unmatched ground truth and detected people. A person 379
 379 (in gt or dt) is defined as a list of keypoint coordinates (if 380
 380 a keypoint is not annotated or detected, the corresponding 381
 381 element in the list is empty). The output of the algorithm is 382
 382 the average precision AP and recall AR.

For single-person settings, the list of matched people 383
 383 consists of the ground-truth annotations and the predicted 384
 384 keypoints. For multiperson settings, a person detector is 385
 385 generally used to compute the people candidates in the scene. 386
 386 In this case, we first carry out a pairing phase to match 387
 387 ground truth and people predictions. We use for this step the 388
 388 pairing algorithm from COCO based on OKS. We set the 389
 389 OKS threshold which controls the pair acceptance to 0 to 390
 390 avoid discarding any person (see [24] for more details).

The calculation of mAPK is carried out as follows. Firstly, 391
 391 we compute a keypoint score KS (Equation 2) for each key- 392
 392 point which is both annotated and detected. A keypoint is 393
 393 considered as correctly detected, *i.e.*, true positive (TP), if 394
 394 its KS score exceeds a threshold selected between 0 and 1. 395
 395 Otherwise, we consider the ground truth and the prediction 396
 396 keypoint unmatched. Then, we count all unmatched keypoint 397
 397 predictions as false positives and unmatched ground-truth 398
 398 keypoints as false negatives. Finally, we compute precision 399
 399 and recall for each type of keypoint. This process is repeated 400
 400 with different acceptance-threshold values (*e.g.*, from 0.5 to 401
 401 0.95, with a step of 0.05) and then averaged to obtain the 402
 402 final performance of the evaluated method.

5. Evaluated Architectures

This section describes the HPE methods in evaluated this 399
 399 study. From the state of the art, we selected three recent net- 400
 400 works.

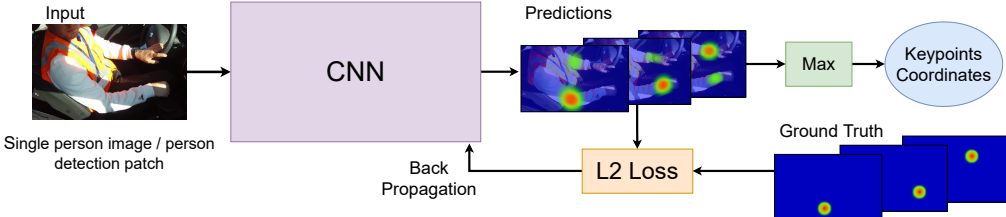


Figure 3: Generic pipeline of HPE methods based on heatmap generation.

Algorithm 1: mAPK computation

Input :

- matched_person*: pairs of (*gt*, *dt*) of matched ground truth and detected people
- unmatched_dts*: unmatched detected people
- unmatched_gts*: unmatched ground-truth people
- acceptance_score*: acceptance-score threshold

Output : AP, AR

```

true_positives=0, false_positives=0, false_negatives = 0
for each (gt, dt) in matched_person do
    for keypoint kp in the skeleton_representation do
        if not empty(dt[kp]) and empty(gt[kp]) then
            false_positives += 1
        else if empty(dt[kp]) and not empty(gt[kp]) then
            false_negatives += 1
        else
            if  $KS(gt[kp], dt[gp]) > acceptance\_score$ 
            then
                true_positives += 1
            else
                false_positives += 1
                false_negatives += 1

    for each keypoint in all unmatched_gts do
        false_negatives += 1
    for each keypoint in all unmatched_dts do
        false_positives += 1
    AP = compute_AP(true_positives, false_positives)
    AR = compute_AR(true_positives, false_negatives)

```

412 tasks. This backbone is based on several convolution layers 413 gathered as blocks, with skip connections between each 414 module adding the input of the module to the output.

415 Xiao *et al.* [39] propose to implement ResNet 50 with a 416 different output module for human pose estimation. First, 417 the ResNet 50 backbone learns to extract the features while 418 reducing the shape of the feature maps. Then, the last stage is 419 composed of three upsampling convolutions combined with 420 BatchNorm [17] and ReLu layers, instead of the original 421 ResNet C5 stage. This deconvolution stage brings back the 422 feature maps to their input size and generates the heatmaps 423 for each keypoint.

424 **5.2. MSPN and RSN**

425 MSPN [22] is a top-down multiperson HPE network. It 426 is built around two steps. First, MegDet [28] object detector 427 identifies the bounding boxes of each person in the images. 428 Then, the picture is cropped around the boxes, and each part 429 serves as input for the multi-stage pose estimator. A stage of 430 the MSPN has a U-shape architecture that processes features 431 at 4 different scales. A bottleneck residual module processes 432 the features at each scale, and skip connections are used 433 between the downsizing stage and its symmetric counterpart 434 in the upsizing stage. Intermediate supervision is applied to 435 each scale of the upsizing stage. Indeed, the loss is applied on 436 heatmaps generated at each scale and which are previously 437 upsampled to the network’s output shape. Stages are then 438 stacked several times (four times in this implementation). 439 To reduce information loss between stages, the architecture 440 uses cross-stage aggregation.

441 works [5, 22, 39] with competitive performances on single 442 and multiperson settings, as discussed in Section 2.2. Using 443 these two categories of methods will allow us to evaluate the 444 relevance of the mAPK metric for both single-person and 445 multiperson settings. These networks are detection-based 446 architectures (Fig. 3). At last, we describe the procedure fol- 447 lowed for training and evaluation of the selected networks. 448

407 **5.1. Simple Baseline ResNet**

408 Simple Baseline (SBI) architecture [39] bases its feature 449 extraction process on the ResNet architecture [14]. ResNet 450 model has been proved well efficient for image-feature ex- 451 traction [32, 2] and is often used in other image processing 452

449 **5.3. Model Training and Inference**

450 The training of the models has been done using the code 451 provided by the respective authors in public repositories, 452 following their recommendations for hyperparameters. All 453

453 training stages were done on the COCO 2017 train set, with 503
454 mini-batches of 32 images and data augmentation operations 504
455 (horizontal flipping, rotation, etc.). The training set is com- 505
456 posed of 118k pictures, while the validation set contains 5k 506
457 images. We used ResNet-50 based Simple Baseline archi- 507
458 tecture, trained for 140 epochs on the COCO dataset with a 508
459 learning rate of 1e-3. RSN and MSPN are trained for 384k 509
460 iterations, with a 5e-4 base learning rate divided by 10 at 510
461 epochs 90 and 120. The networks were trained on two 24GB 511
462 Nvidia Titan RTX with 64GB of RAM and an Intel i9900k 512
463 processor. 513

464 Also, since DriPE is a single-person dataset, all network 514
465 models took as input the full image. However, for COCO 515
466 which is a multiperson dataset, the models took as input 516
467 a patch cropped around the output of a person detection 517
468 algorithm. 518

469 6. Results and Discussion

470 We first present the performance of the three described 520
471 networks trained on COCO 2017 and tested on both the 521
472 COCO validation set and the DriPE test set. Then, we present 522
473 the results of these models after finetuning them on the 523
474 training set of DriPE dataset. We first use AP metric based 524
475 on OKS, then compare the results with mAPK metric results. 525

476 6.1. Performance of Networks trained on COCO 526 477 Dataset 527

478 This evaluation studies the performance of the trained 529
479 networks on the COCO validation set (Table 2) using the 530
480 official dataset evaluation procedure. We validate that the 531
481 trained models achieves a performance close to the original 532
482 work (around 2% less on average). 533

483 Then, we evaluate the performance of these methods 534
484 on DriPE test set (Table 3) using the models trained on 535
485 COCO 2017. Due to the camera placement in the car, DriPE 536
486 contains only "Large" subjects (subjects with a bounding 537
487 box containing more than 96^2 pixels [24]). Therefore, it is 538
488 more suitable to compare COCO and DriPE datasets using 539
489 AP^L and AR^L column values. 540

490 The state-of-the-art networks show slightly lower perfor- 541
491 mances on DriPE dataset than on the COCO dataset (Tables 2 542
492 and 3). On one hand, we note that on average, AP^L and 543
493 AR^L are lower on DriPE than on COCO. On another hand, 544
494 we observe higher precision and recall scores on the three 545
495 networks when using an OKS threshold of 50% (AP⁵⁰) or 546
496 75% threshold (AP⁷⁵). The results suggest that most of the 547
497 improvements to be made in the car context concern the pre- 548
498 cision of the localization of keypoint predictions (AR / AP 549
499 threshold superior to 75 %). 550

500 6.2. Finetuning on DriPE Dataset

501 We finetune the three networks on DriPE training set. 553
502 Finetuning has been done for 10 epochs with a learning rate 554

10 times lower than the original learning rate used for the
COCO base training (Table 4).

Results indicate a gain from 20 to 25% in AP and 10 to 15% in AR after finetuning the networks. This increase can be partially explained by the relatively small variance of the dataset. Therefore, the networks could have overfitted the training set without experiencing an important performance loss on the test set. Despite that, the improvement of performance suggests that the networks learned specific features on DriPE that they did not learn on a general dataset, which highlights the relevance of DriPE dataset to the field. Eventually, AP OKS results may suggest that HPE inside of a car cockpit would be a nearly solved problem, at least when evaluating the performance of keypoint detections methods at a people level.

518 6.3. Comparison with mAPK Metric

519 This evaluation assesses the performance of the same
models but at the level of keypoint predictions. We recomputed
520 the performance of the evaluated models (Tables 2 and
521 3) using mAPK metric (Table 5 and Table 6).

522 We observe that even if AP OKS and mAPK metrics
values are not directly comparable, the recall scores are close
523 between the two metrics (around 75%) (Tables 2, 3, 5, and 6).
524 However, we note that the average precision scores are lower
with mAPK. This decay in precision is explained by the high
525 number of false positives that are considered by mAPK but
ignored by OKS (Table 7). After analysis, we determined
526 that most of the false positives come from the non-annotated
527 points, particularly for the MSPN and RSN architectures.
528 These results show that the networks are overconfident in
529 their prediction and cannot properly detect the absence of
530 a keypoint on the image. Note that this information cannot
531 be found with AP OKS since the score is not computed at a
532 keypoint level.

533 It is worth noticing that even if the head keypoints are
534 considered as some of the easiest keypoints to detect in HPE,
535 trained models have attained a very low average precision
536 on their detection. The overall number of false positives
537 is almost twice higher than the number of true positives
538 (Table 7). In fact, the COCO annotation policy does not
539 annotate occluded keypoints on the head. Therefore, these
540 results highlight that the current models have difficulties
541 not detecting keypoints, *i.e.*, to identify when a keypoint
542 is not visible. Also, the models on DriPE have very low
543 performance on ankles detection, both in precision and recall.
544 The ankles are usually difficult to predict, particularly inside
545 of a car, where the lower limbs are almost totally occluded by
546 the dashboard. This occlusion difficulty paired up with the
547 low contrast and luminosity makes the detection of ankles
548 very challenging.

549 Finally, we compare the evaluation of the finetuned net-
550 work using mAPK (Table 8). First, we may observe that

555 this metric confirms the increase of prediction performances
 556 indicated by AP OKS (Table 4). Then, we notice that the
 557 precision did not increase as much as the recall. These
 558 results highlight the importance of DriPE to improve the
 559 performance of current models on monitoring people in the
 560 consumer car context. But they also bring attention to open
 561 challenges on keypoint prediction that cannot be solved by
 562 simply finetuning the current models on a dataset-specific
 563 task. Astonishingly, Simple Baseline ranks higher than more
 564 recent methods according to mAPK. This can be observed
 565 on both datasets and it is especially true for precision values.
 566 It reveals that Simple Baseline has a lower number of
 567 false positives, which shows a better ability to not predict
 568 non-annotated keypoints.

569 7. Conclusion and Perspectives

570 This paper has presented two contributions: firstly, a
 571 new keypoint-based metric, named mAPK, to measure the
 572 performance of HPE methods. Secondly, a novel dataset,
 573 named DriPE, to benchmark methods for monitoring the
 574 pose of drivers in consumer vehicles. The mAPK metric is
 575 an extension of APK and OKS evaluation metrics. Results
 576 indicate it characterizes more precisely the performance of
 577 HPE methods in terms of keypoint detection, both on general
 578 and driving datasets.

579 The DriPE dataset is the first publicly available dataset
 580 depicting images of drivers in real-world conditions. We
 581 have shown that it may contribute to further improve the per-
 582 formance of deep neural networks on the driver monitoring
 583 task. Moreover, the mAPK metric indicates that simply fine-
 584 tuning current methods on the DriPE dataset is insufficient to
 585 fully address the driver monitoring task. These results imply
 586 that more precise methods must be developed to tackle the
 587 existing challenges.

588 Future work will investigate how to include other evalua-
 589 tion aspects in the proposed metric. For instance, the impact
 590 of the confidence threshold on the measured performance.
 591 Also, the proposed metric ignores the varying difficulty of
 592 predicting keypoints of different limbs and treats equally
 593 keypoints of different levels of visibility. Predicting the visi-
 594 bility of keypoints could provide interesting information for
 595 a spatial understanding of the interactions of the person with
 596 the scene.

597 Acknowledgements

598 This work was supported by the Pack Ambition
 599 Recherche 2019 funding of the French AURA Region in
 600 the context of the AutoBehave project.

AP OKS (%)	AP	AP ⁵⁰	AP ⁷⁵	AP ^L	AR	AR ⁵⁰	AR ⁷⁵	AR ^L
SBI [39]	72	92	80	77	76	93	82	80
MSPN [22]	77	94	85	82	80	95	87	85
RSN [5]	76	94	84	81	79	94	85	84

Table 2: HPE on the COCO 2017 validation set.

AP OKS (%)	AP	AP ⁵⁰	AP ⁷⁵	AP ^L	AR	AR ⁵⁰	AR ⁷⁵	AR ^L
SBI [39]	75	99	91	75	81	99	94	81
MSPN [22]	81	99	97	81	85	99	97	85
RSN [5]	75	99	93	75	79	99	95	79

Table 3: HPE on the DriPE test set.

AP OKS (%)	AP	AP ⁵⁰	AP ⁷⁵	AP ^L	AR	AR ⁵⁰	AR ⁷⁵	AR ^L
SBI [39]	97	100	80	97 ↑	97	100	99	99
MSPN [22]	97	100	99	97 ↑	98	100	99	98
RSN [5]	91	99	98	91↑	94	100	99	94

Table 4: HPE of finetuned networks on the DriPE test set.

mAPK (%)	Head	Sho.	Elb.	Wri.	Hip	Knee	Ank.	Mean
AP	SBI [39]	44	69	59	55	65	62	60
	MSPN [22]	49	76	60	53	62	47	40
	RSN [5]	49	76	59	52	61	46	39
AR	SBI [39]	82	86	83	79	80	81	80
	MSPN [22]	87	88	87	84	82	85	85
	RSN [5]	86	88	86	83	82	84	85

Table 5: HPE on the COCO 2017 validation set.

mAPK (%)	Head	Sho.	Elb.	Wri.	Hip	Knee	Ank.	Mean
AP	SBI [39]	29	86	78	92	91	75	14
	MSPN [22]	25	80	77	90	91	77	13
	RSN [5]	25	78	76	89	88	68	11
AR	SBI [39]	89	92	93	96	88	61	09
	MSPN [22]	96	87	96	97	92	77	45
	RSN [5]	94	85	95	96	89	68	33

Table 6: HPE on the DriPE test set.

	Head	Should.	Elbow	Wrist	Hip	Knee	Ankle	Total
GT	17k	25k	21k	26k	26k	26k	11k	152k
TP	16k	21k	20k	23k	23k	18k	2.8k	124k
FP	50k	5.7k	6.4k	3.1k	3.1k	8.4k	24k	100k
FN	0.7k	3.8k	1.1k	2.9k	3.0k	8.3k	8.2k	28k

Table 7: Performance of RSN model on DriPE test set with mAPK metric.

	Head	Should.	Elbow	Wrist	Hip	Knee	Ank.	Mean
AP	SBI [39]	24	90	79	94	98	98	40
	MSPN [22]	25	89	79	91	97	94	38
	RSN [5]	25	88	78	91	95	86	30
AR	SBI [39]	93	97	98	98	98	98	94
	MSPN [22]	97	97	98	99	98	94	87
	RSN [5]	91	95	98	98	95	86	73

Table 8: HPE on the DriPE test set of finetuned networks.

601 References

- [1] Mykhaylo Andriluka, Leonid Pishchulin, Peter Gehler, and Bernt Schiele. 2d human pose estimation: New benchmark

- 604 and state of the art analysis. In *IEEE Conference on Computer Vision and Pattern Recognition (CVPR)*, June 2014. 1, 2, 3 661
- 605 [2] Bruno Artacho and Andreas Savakis. Unipose: Unified hu- 663
- 606 man pose estimation in single images and videos. In *Proceed- 664*
- 607 *ings of the IEEE/CVF Conference on Computer Vision and 665*
- 608 *Pattern Recognition (CVPR)*, pages 7035–7044, 2020. 3, 5, 6 666
- 609 [3] Guido Borghi, Stefano Pini, Roberto Vezzani, and Rita Cuc- 667
- 610 chiara. Mercury: a vision-based framework for driver mon- 668
- 611 itoring. In *International Conference on Intelligent Human 669*
- 612 *Systems Integration*, pages 104–110. Springer, 2020. 2 670
- 613 [4] Guido Borghi, Marco Venturelli, Roberto Vezzani, and Rita 671
- 614 Cucchiara. Poseidon: Face-from-depth for driver pose esti- 672
- 615 *mation*. In *Proceedings of the IEEE conference on computer 673*
- 616 *vision and pattern recognition*, pages 4661–4670, 2017. 2 674
- 617 [5] Yuanhao Cai, Zhicheng Wang, Zhengxiong Luo, Binyi Yin, 675
- 618 Angang Du, Haoqian Wang, Xinyu Zhou, Erjin Zhou, Xi- 676
- 619 angyu Zhang, and Jian Sun. Learning delicate local represen- 677
- 620 tations for multi-person pose estimation. In *ECCV*, 2020. 3, 678
- 621 6, 8
- 622 [6] Zhe Cao, Gines Hidalgo, Tomas Simon, Shih-En Wei, and 679
- 623 Yaser Sheikh. Openpose: realtime multi-person 2d pose 680
- 624 estimation using part affinity fields. *IEEE transactions on 681*
- 625 *pattern analysis and machine intelligence*, 43(1):172–186, 682
- 626 2019. 2
- 627 [7] Zhe Cao, Tomas Simon, Shih-En Wei, and Yaser Sheikh. 683
- 628 Realtime multi-person 2d pose estimation using part affinity 684
- 629 fields. In *Proceedings of the IEEE Conference on Computer 685*
- 630 *Vision and Pattern Recognition (CVPR)*, July 2017. 3 686
- 631 [8] Joao Carreira, Pulkit Agrawal, Katerina Fragkiadaki, and Ji- 687
- 632 tendra Malik. Human pose estimation with iterative error 688
- 633 feedback. In *Proceedings of the IEEE Conference on Com- 689*
- 634 *puter Vision and Pattern Recognition (CVPR)*, June 2016. 690
- 635 2
- 636 [9] Yu Chen, Chunhua Shen, Xiu-Shen Wei, Lingqiao Liu, and 691
- 637 Jian Yang. Adversarial posenet: A structure-aware convolu- 692
- 638 tional network for human pose estimation. In *Proceedings 693*
- 639 *of the IEEE International Conference on Computer Vision 694*
- 640 *(ICCV)*, Oct 2017. 3 695
- 641 [10] Yilun Chen, Zhicheng Wang, Yuxiang Peng, Zhiqiang Zhang, 696
- 642 Gang Yu, and Jian Sun. Cascaded pyramid network for multi- 697
- 643 person pose estimation. In *Proceedings of the IEEE Confer- 698*
- 644 *ence on Computer Vision and Pattern Recognition (CVPR)*, 699
- 645 June 2018. 3
- 646 [11] Xiao Chu, Wei Yang, Wanli Ouyang, Cheng Ma, Alan L. 700
- 647 Yuille, and Xiaogang Wang. Multi-context attention for hu- 701
- 648 man pose estimation. In *Proceedings of the IEEE Conference 702*
- 649 *on Computer Vision and Pattern Recognition (CVPR)*, July 703
- 650 2017. 3
- 651 [12] Marcin Eichner, Manuel Marin-Jimenez, Andrew Zisserman, 704
- 652 and Vittorio Ferrari. 2d articulated human pose estimation and 705
- 653 retrieval in (almost) unconstrained still images. *International 706*
- 654 *Journal of Computer Vision*, 99(2):190–214, 2012. 1, 3 707
- 655 [13] Hartmut Feld, Bruno Mirbach, Jigyasa Singh Katrolia, Mo- 708
- 656 hamed Selim, Oliver Wasenmüller, and Didier Stricker. Dfki 709
- 657 cabin simulator: A test platform for visual in-cabin mon- 710
- 658 itoring functions. In *Proceedings of the 6th Commercial 711*
- 659 *Vehicle Technology Symposium (CVT)*, 6th International, Uni- 712
- 660 versity of Kaiserslautern, 2020. University of Kaiserslautern, 713
- 661 Springer. 2
- [14] Kaiming He, Xiangyu Zhang, Shaoqing Ren, and Jian Sun. 714
- Deep residual learning for image recognition. In *Proceedings 715*
- 716 *of the IEEE Conference on Computer Vision and Pattern 717*
- 718 *Recognition (CVPR)*, June 2016. 3, 6
- [15] Kaiming He, Xiangyu Zhang, Shaoqing Ren, and Jian Sun. 719
- Deep residual learning for image recognition. In *Proceedings 720*
- 721 *of the IEEE Conference on Computer Vision and Pattern 722*
- 723 *Recognition (CVPR)*, June 2016. 3
- [16] Gines Hidalgo, Yaadhav Raaj, Haroon Idrees, Donglai Xi- 724
- 725 ang, Hanbyul Joo, Tomas Simon, and Yaser Sheikh. Single- 726
- 727 network whole-body pose estimation. In *Proceedings of the 728*
- 729 *IEEE/CVF International Conference on Computer Vision*, 730
- 731 pages 6982–6991, 2019. 2
- [17] Sergey Ioffe and Christian Szegedy. Batch normalization: 732
- Accelerating deep network training by reducing internal co- 733
- variate shift. *CoRR*, abs/1502.03167, 2015. 6
- [18] Imen Jegham, Anouar Ben Khalifa, Ihssen Alouani, and Mo- 734
- 735 hammed Ali Mahjoub. Mdad: A multimodal and multiview 736
- 737 in-vehicle driver action dataset. In *International Conference 738*
- 739 *on Computer Analysis of Images and Patterns*, pages 518–529. 740
- 741 Springer, 2019. 2
- [19] Sam Johnson and Mark Everingham. Clustered pose and 742
- 743 nonlinear appearance models for human pose estimation. In 744
- 744 *Proceedings of the British Machine Vision Conference*, 2010. 745
- 745 doi:10.5244/C.24.12. 1, 2, 5
- [20] Lipeng Ke, Ming-Ching Chang, Honggang Qi, and Siwei 746
- 747 Lyu. Multi-scale structure-aware network for human pose 748
- 749 estimation. In *Proceedings of the European Conference on 750*
- 750 *Computer Vision (ECCV)*, September 2018. 3, 5
- [21] Alex Krizhevsky, Ilya Sutskever, and Geoffrey E Hinton. 751
- 752 Imagenet classification with deep convolutional neural networks. 753
- In F. Pereira, C. J. C. Burges, L. Bottou, and K. Q. Weinberger, 754
- editors, *Advances in Neural Information Processing Systems* 755
- 25, pages 1097–1105. Curran Associates, Inc., 2012. 2
- [22] Wenbo Li, Zhicheng Wang, Binyi Yin, Qixiang Peng, 756
- Yuming Du, Tianzi Xiao, Gang Yu, Hongtao Lu, Yichen 757
- Wei, and Jian Sun. Rethinking on multi-stage networks 758
- 759 for human pose estimation. <https://github.com/megvii-detection/MSPN.git>, 2019. 3, 6, 8
- [23] Tsung-Yi Lin, Piotr Dollar, Ross Girshick, Kaiming He, 760
- Bharath Hariharan, and Serge Belongie. Feature pyramid 761
- 762 networks for object detection. In *Proceedings of the IEEE 763*
- 763 *Conference on Computer Vision and Pattern Recognition (CVPR)*, 764
- 764 July 2017. 3
- [24] Tsung-Yi Lin, Michael Maire, Serge Belongie, Lubomir Bour- 765
- dev, Ross Girshick, James Hays, Pietro Perona, Deva Ra- 766
- manan, C. Lawrence Zitnick, and Piotr Dollár. Microsoft 767
- coco: Common objects in context, 2015. 1, 2, 3, 5, 7
- [25] Manuel Martin, Alina Roitberg, Monica Haurilet, Matthias 768
- Horne, Simon Reiß, Michael Voit, and Rainer Stiefelhagen. 769
- Drive&act: A multi-modal dataset for fine-grained driver 770
- behavior recognition in autonomous vehicles. In *The IEEE 771*
- 772 *International Conference on Computer Vision (ICCV)*, Oct 773
- 773 2019. 2, 4

- 717 [26] Alejandro Newell, Zhiao Huang, and Jia Deng. Associative 775
718 embedding: End-to-end learning for joint detection and group- 776
719 ing. In I. Guyon, U. V. Luxburg, S. Bengio, H. Wallach, R. 777
720 Fergus, S. Vishwanathan, and R. Garnett, editors, *Advances in 778*
721 *Neural Information Processing Systems 30*, pages 2277–2287. 779
722 Curran Associates, Inc., 2017. 3 780
- 723 [27] Alejandro Newell, Kaiyu Yang, and Jia Deng. Stacked Hour- 781
724 glass Networks for Human Pose Estimation. In Bastian Leibe, 782
725 Jiri Matas, Nicu Sebe, and Max Welling, editors, *Computer 783*
726 *Vision – ECCV 2016*, pages 483–499, Cham, 2016. Springer 784
727 International Publishing. 3, 4
- 728 [28] Chao Peng, Tete Xiao, Zeming Li, Yuning Jiang, Xiangyu 785
729 Zhang, Kai Jia, Gang Yu, and Jian Sun. Megdet: A large mini- 786
730 batch object detector. In *Proceedings of the IEEE Conference 787*
731 *on Computer Vision and Pattern Recognition*, pages 6181– 788
732 6189, 2018. 6
- 733 [29] Shaoqing Ren, Kaiming He, Ross Girshick, and Jian Sun. 789
734 Faster r-cnn: Towards real-time object detection with region 790
735 proposal networks. In C. Cortes, N. D. Lawrence, D. D. Lee, 791
736 M. Sugiyama, and R. Garnett, editors, *Advances in Neural 792*
737 *Information Processing Systems 28*, pages 91–99. Curran 793
738 Associates, Inc., 2015. 3
- 739 [30] Benjamin Sapp and Ben Taskar. Modec: Multimodal decom- 794
740 posable models for human pose estimation. In *Proceedings 795*
741 *of the IEEE Conference on Computer Vision and Pattern 796*
742 *Recognition (CVPR)*, 2013. 1, 2
- 743 [31] Ke Sun, Bin Xiao, Dong Liu, and Jingdong Wang. Deep high- 797
744 resolution representation learning for human pose estimation. 798
745 In *Proceedings of the IEEE/CVF Conference on Computer 799*
746 *Vision and Pattern Recognition (CVPR)*, June 2019. 3
- 747 [32] Xiao Sun, Jiaxiang Shang, Shuang Liang, and Yichen Wei. 800
748 Compositional human pose regression. In *Proceedings of the 801*
749 *IEEE International Conference on Computer Vision (ICCV)*, 802
750 Oct 2017. 2, 6
- 751 [33] Christian Szegedy, Wei Liu, Yangqing Jia, Pierre Sermanet, 803
752 Scott Reed, Dragomir Anguelov, Dumitru Erhan, Vincent 804
753 Vanhoucke, and Andrew Rabinovich. Going deeper with 805
754 convolutions. In *Proceedings of the IEEE Conference on 806*
755 *Computer Vision and Pattern Recognition (CVPR)*, June 2015. 807
756 2
- 757 [34] Wei Tang and Ying Wu. Does learning specific features for 808
758 related parts help human pose estimation? In *Proceedings of 809*
759 *the IEEE/CVF Conference on Computer Vision and Pattern 810*
760 *Recognition (CVPR)*, June 2019. 3, 5
- 761 [35] Wei Tang, Pei Yu, and Ying Wu. Deeply learned composi- 811
762 tional models for human pose estimation. In *Proceedings 812*
763 *of the European Conference on Computer Vision (ECCV)*, 813
764 September 2018. 3, 4
- 765 [36] A. Toshev and C. Szegedy. Deeppose: Human pose estima- 814
766 tion via deep neural networks. In *2014 IEEE Conference on 815*
767 *Computer Vision and Pattern Recognition*, pages 1653–1660, 816
768 2014. 2
- 769 [37] Zhou Wang, Alan C Bovik, Hamid R Sheikh, and Eero P 817
770 Simoncelli. Image quality assessment: from error visibility to 818
771 structural similarity. *IEEE transactions on image processing*, 819
772 13(4):600–612, 2004. 4
- 773 [38] Shih-En Wei, Varun Ramakrishna, Takeo Kanade, and Yaser 820
774 Sheikh. Convolutional pose machines. In *Proceedings of the 821*
- IEEE Conference on Computer Vision and Pattern Recognition (CVPR), June 2016. 4
- [39] Bin Xiao, Haiping Wu, and Yichen Wei. Simple baselines for human pose estimation and tracking. In *Proceedings of the European Conference on Computer Vision (ECCV)*, September 2018. 2, 3, 4, 5, 6, 8
- [40] Yi Yang and Deva Ramanan. Articulated human detection with flexible mixtures of parts. *IEEE transactions on pattern analysis and machine intelligence*, 35(12):2878–2890, 2012. 1, 3, 5